

Indication for the disappearance of reactor $\bar{\nu}_e$ in the Double Chooz experiment

Y. Abe,²⁸ C. Aberle,²¹ T. Akiri,^{4,15} J.C. dos Anjos,⁵ F. Ardellier,¹⁵ A.F. Barbosa,^{5,*} A. Baxter,²⁶ M. Bergevin,⁹ A. Bernstein,¹⁶ T.J.C. Bezerra,³⁰ L. Bezrukhov,¹⁴ E. Blucher,⁶ M. Bongrand,^{15,30} N.S. Bowden,¹⁶ C. Buck,²¹ J. Busenitz,² A. Cabrera,⁴ E. Caden,¹⁰ L. Camilleri,⁸ R. Carr,⁸ M. Cerrada,⁷ P.-J. Chang,¹⁷ P. Chimenti,³⁴ T. Classen,^{9,16} A.P. Collin,¹⁵ E. Conover,⁶ J.M. Conrad,²⁰ S. Cormon,²⁵ J.I. Crespo-Anadón,⁷ M. Cribier,^{15,4} K. Crum,⁶ A. Cucoanes,^{25,15} M.V. D'Agostino,³ E. Damon,¹⁰ J.V. Dawson,^{4,36} S. Dazeley,¹⁶ M. Dierckxsens,⁶ D. Dietrich,³³ Z. Djurcic,³ M. Dracos,²⁴ V. Durand,^{15,4} Y. Efremenko,²⁷ M. Elnimr,²⁵ Y. Endo,²⁹ A. Etenko,¹⁹ E. Falk,²⁶ M. Fallot,²⁵ M. Fechner,¹⁵ F. von Feilitzsch,³¹ J. Felde,⁹ S.M. Fernandes,²⁶ D. Franco,⁴ A.J. Franke,⁸ M. Franke,³¹ H. Furuta,³⁰ R. Gama,⁵ I. Gil-Botella,⁷ L. Giot,²⁵ M. Göger-Neff,³¹ L.F.G. Gonzalez,³⁵ M.C. Goodman,³ J.T.M. Goon,² D. Greiner,³³ B. Guillon,²⁵ N. Haag,³¹ C. Hagner,¹¹ T. Hara,¹⁸ F.X. Hartmann,²¹ J. Hartnell,²⁶ T. Haruna,²⁹ J. Haser,²¹ A. Hatzikoutelis,²⁷ T. Hayakawa,^{22,15} M. Hofmann,³¹ G.A. Horton-Smith,¹⁷ M. Ishitsuka,²⁸ J. Jochum,³³ C. Jollet,²⁴ C.L. Jones,²⁰ F. Kaether,²¹ L. Kalousis,²⁴ Y. Kamyshev,²⁷ D.M. Kaplan,¹³ T. Kawasaki,²² G. Keefer,¹⁶ E. Kemp,³⁵ H. de Kerret,^{4,36} Y. Kibe,²⁸ T. Konno,²⁸ D. Kryn,⁴ M. Kuze,²⁸ T. Lachenmaier,³³ C.E. Lane,¹⁰ C. Langbrandtner,²¹ T. Lasserre,^{15,4} A. Letourneau,¹⁵ D. Lhuillier,¹⁵ H.P. Lima Jr,⁵ M. Lindner,²¹ Y. Liu,² J.M. López-Castanõ,⁷ J.M. LoSecco,²³ B.K. Lubsandorzhiev,¹⁴ S. Lucht,¹ D. McKee,^{2,17} J. Maeda,²⁹ C.N. Maesano,⁹ C. Mariani,⁸ J. Maricic,¹⁰ J. Martino,²⁵ T. Matsubara,²⁹ G. Mention,¹⁵ A. Meregaglia,²⁴ T. Miletic,¹⁰ R. Milincic,¹⁰ A. Milzstajn,^{15,*} H. Miyata,²² D. Motta,^{15,*} Th.A. Mueller,^{15,30} Y. Nagasaka,¹² K. Nakajima,²² P. Novella,⁷ M. Obolensky,⁴ L. Oberauer,³¹ A. Onillon,²⁵ A. Osborn,²⁷ I. Ostrovskiy,² C. Palomares,⁷ S.J.M. Peeters,²⁶ I.M. Pepe,⁵ S. Perasso,¹⁰ P. Perrin,¹⁵ P. Pfahler,³¹ A. Porta,²⁵ W. Potzel,³¹ R. Queval,¹⁵ J. Reichenbacher,² B. Reinhold,²¹ A. Remoto,^{25,4} D. Reyna,³ M. Röhling,³³ S. Roth,¹ H.A. Rubin,¹³ Y. Sakamoto,³² R. Santorelli,⁷ F. Sato,²⁹ S. Schönert,³¹ S. Schoppmann,¹ U. Schwan,²¹ T. Schwetz,²¹ M.H. Shaevitz,⁸ D. Shrestha,¹⁷ J-L. Sida,¹⁵ V. Sinev,^{14,15} M. Skorokhvatov,¹⁹ E. Smith,¹⁰ J. Spitz,²⁰ A. Stahl,¹ I. Stancu,² M. Strait,⁶ A. Stüken,¹ F. Suekane,³⁰ S. Sukhotin,¹⁹ T. Sumiyoshi,²⁹ Y. Sun,² Z. Sun,¹⁵ R. Svoboda,⁹ H. Tabata,³⁰ N. Tamura,²² K. Terao,²⁰ A. Tonazzo,⁴ M. Touns,⁸ H.H. Trinh Thi,³¹ C. Veyssiere,¹⁵ S. Wagner,²¹ H. Watanabe,²¹ B. White,²⁷ C. Wiebusch,¹ L. Winslow,²⁰ M. Worcester,⁶ M. Wurm,¹¹ E. Yanovitch,¹⁴ F. Yermia,²⁵ K. Zbiri,^{25,10} and V. Zimmer³¹

(Double Chooz Collaboration)

¹III. Physikalisches Institut, RWTH Aachen University, 52056 Aachen, Germany

²Department of Physics and Astronomy, University of Alabama, Tuscaloosa, Alabama 35487, USA

³Argonne National Laboratory, Argonne, Illinois 60439, USA

⁴APC, AstroParticule et Cosmologie, Université Paris Diderot, CNRS/IN2P3, CEA/IRFU, Observatoire de Paris, Sorbonne Paris Cité, 75205 Paris Cedex 13, France

⁵Centro Brasileiro de Pesquisas Físicas, Rio de Janeiro, RJ, cep 22290-180, Brazil

⁶The Enrico Fermi Institute, The University of Chicago, Chicago, IL 60637, USA

⁷Centro de Investigaciones Energéticas, Medioambientales y Tecnológicas, CIEMAT, E-28040, Madrid, Spain

⁸Columbia University; New York, NY 10027, USA

⁹University of California, Davis, CA-95616-8677, USA

¹⁰Physics Department, Drexel University, Philadelphia, Pennsylvania 19104, USA

¹¹Institut für Experimentalphysik, Universität Hamburg, 22761 Hamburg, Germany

¹²Hiroshima Institute of Technology, Hiroshima, 731-5193, Japan

¹³Department of Physics, Illinois Institute of Technology, Chicago, Illinois 60616, USA

¹⁴Institute of Nuclear Research of the Russian Academy of Science, Russia

¹⁵Commissariat à l'Energie Atomique et aux Energies Alternatives, Centre de Saclay, IRFU, 91191 Gif-sur-Yvette, France

¹⁶Lawrence Livermore National Laboratory, Livermore, CA 94550, USA

¹⁷Department of Physics, Kansas State University, Manhattan, Kansas 66506, USA

¹⁸Department of Physics, Kobe University, Kobe, 657-8501, Japan

¹⁹NRC Kurchatov Institute, 123182 Moscow, Russia

²⁰Massachusetts Institute of Technology; Cambridge, MA 02139, USA

²¹Max-Planck-Institut für Kernphysik, 69029 Heidelberg, Germany

²²Department of Physics, Niigata University, Niigata, 950-2181, Japan

²³University of Notre Dame, Notre Dame, IN 46556-5670, USA

²⁴IPHC, Université de Strasbourg, CNRS/IN2P3, F-67037 Strasbourg, France

²⁵SUBATECH, CNRS/IN2P3, Université de Nantes, Ecole des Mines de Nantes, F-44307 Nantes, France

²⁶Department of Physics and Astronomy, University of Sussex, Falmer, Brighton BN1 9QH, United Kingdom

²⁷Department of Physics and Astronomy, University of Tennessee, Knoxville, Tennessee 37996, USA

²⁸Department of Physics, Tokyo Institute of Technology, Tokyo, 152-8551, Japan

²⁹Department of Physics, Tokyo Metropolitan University, Tokyo, 192-0397, Japan

³⁰Research Center for Neutrino Science, Tohoku University, Sendai 980-8578, Japan

³¹Physik Department, Technische Universität München, 85747 Garching, Germany

³²Tohoku Gakuin University, Sendai, 981-3193, Japan

³³Kepler Center for Astro and Particle Physics, Universität Tübingen, 72076, Tübingen, Germany

³⁴Universidade Federal do ABC, UFABC, Sao Paulo, Santo André, SP, Brazil

³⁵Universidade Estadual de Campinas-UNICAMP, Campinas, SP, Brazil

³⁶Laboratoire Neutrino de Champagne Ardenne, domaine d'Aviette, 08600 Rancennes, France

(Dated: March 15, 2012)

The Double Chooz Experiment presents an indication of reactor electron antineutrino disappearance consistent with neutrino oscillations. An observed-to-predicted ratio of events of 0.944 ± 0.016 (stat) ± 0.040 (syst) was obtained in 101 days of running at the Chooz Nuclear Power Plant in France, with two 4.25 GW_{th} reactors. The results were obtained from a single 10 m³ fiducial volume detector located 1050 m from the two reactor cores. The reactor antineutrino flux prediction used the Bugey4 flux measurement after correction for differences in core composition. The deficit can be interpreted as an indication of a non-zero value of the still unmeasured neutrino mixing parameter $\sin^2 2\theta_{13}$. Analyzing both the rate of the prompt positrons and their energy spectrum we find $\sin^2 2\theta_{13} = 0.086 \pm 0.041$ (stat) ± 0.030 (syst), or, at 90% CL, $0.017 < \sin^2 2\theta_{13} < 0.16$.

PACS numbers: 14.60.Pq, 13.15.+g, 25.30.Pt, 95.55.Vj, 28.41.Ak

Keywords: neutrino oscillations, neutrino mixing, reactor

We report first results of a search for a non-zero neutrino oscillation [1] mixing angle, θ_{13} , based on reactor antineutrino disappearance. This is the last of the three neutrino oscillation mixing angles [2, 3] for which only upper limits [4, 5] are available. The size of θ_{13} sets the required sensitivity of long-baseline oscillation experiments attempting to measure CP violation in the neutrino sector or the mass hierarchy.

In reactor experiments [6, 7] addressing the disappearance of $\bar{\nu}_e$, θ_{13} determines the survival probability of electron antineutrinos at the “atmospheric” squared-mass difference, Δm_{atm}^2 . This probability is given by:

$$P_{surv} \approx 1 - \sin^2 2\theta_{13} \sin^2(1.267 \Delta m_{atm}^2 L/E), \quad (1)$$

where L is the distance from reactor to detector in meters and E the energy of the antineutrino in MeV. The full formula can be found in Ref. [1]. Eq. 1 provides a direct way to measure θ_{13} since the only additional input is the well measured value of $|\Delta m_{atm}^2| = (2.32_{-0.08}^{+0.12}) \times 10^{-3} \text{ eV}^2$ [8]. Other running reactor experiments [9, 10] are using the same technique.

Electron antineutrinos of < 9 MeV are produced by reactors and detected through inverse beta decay (IBD): $\bar{\nu}_e + p \rightarrow e^+ + n$. Detectors based on hydrocarbon liquid scintillators provide the free proton targets. The IBD signature is a coincidence of a prompt positron signal followed by a delayed neutron capture. The $\bar{\nu}_e$ energy, $E_{\bar{\nu}_e}$, is reconstructable from E_{prompt} , the positron visible energy ($E_{\bar{\nu}_e} \cong E_{prompt} + 0.78 \text{ MeV}$).

Recently, indications of non-zero θ_{13} have been reported by two accelerator appearance experiments: T2K [11] and MINOS [12]. Global fits (see e.g. [13, 14]) indicate central values in the range

$0.05 < \sin^2 2\theta_{13} < 0.10$, accessible to the Double Chooz experiment [15, 16].

We present here our first results with a detector located ~ 1050 m from the two 4.25 GW_{th} thermal power reactors of the Chooz Nuclear Power Plant and under a 300 MWE rock overburden. The analysis is based on 101 days of data including 16 days with one reactor off and one day with both reactors off.

The antineutrino flux of each reactor depends on its thermal power and, for the four main fissioning isotopes, ²³⁵U, ²³⁹Pu, ²³⁸U, ²⁴¹Pu, their fraction of the total fuel content, their energy released per fission, and their fission and capture cross-sections. The fission rates and associated errors were evaluated using two predictive and complementary reactor simulation codes: MURE [17, 18] and DRAGON [19]. This allowed a study of the sensitivity to the important reactor parameters (e.g., thermal power, boron concentration, temperatures and densities). The quality of these simulations was evaluated through benchmarks [20], and comparisons with Electricité de France (EDF) assembly simulations. The maximum discrepancies observed were included in the fission rate systematic error.

MURE was used to develop a 3D simulation of the reactor cores. EDF provided the information required to simulate the fission rates including initial burnups of assemblies. To determine the inventories of each assembly composing the core at the startup of the data-taking cycle, assembly simulations were performed and the inventories at the given burnup computed. The energies per fission computed by Kopeikin [21] and nuclear data evaluated from the JEFF3.1 database [22] were used. The evolutions of the core simulations with time were performed using the thermal power and the boron concentration from the EDF database averaged over 48 h time steps, yielding the relative contributions to fissions of the four main isotopes.

The associated antineutrino flux was computed using

* Deceased.

the improved spectra from [23], converted from the ILL reference electron spectra [24–26], and the updated *ab initio* calculation of the ^{238}U spectrum [27]. The ILL spectra were measured after irradiating U or Pu for ~ 1 day. Contributions from β -decays with lifetimes longer than these irradiation times were accounted for as prescribed in [27].

The Double Chooz detector system (Figure 1) consists of a main detector, an outer veto, and calibration devices. The main detector comprises four concentric cylindrical tanks filled with liquid scintillators or mineral oil. The innermost 8 mm thick transparent (UV to visible) acrylic vessel houses the 10 m^3 ν -target liquid, a mixture of n-dodecane, PXE, PPO, bis-MSB and 1 g gadolinium/l as a beta-diketonate complex. The scintillator choice emphasizes radiopurity and long term stability [28]. The ν -target volume is surrounded by the γ -catcher, a 55 cm thick Gd-free liquid scintillator layer in a second 12 mm thick acrylic vessel, used to detect γ -rays escaping from the ν -target. The light yield of the γ -catcher was chosen to provide identical photoelectron (pe) yield across these two layers [29]. Outside the γ -catcher is the buffer, a 105 cm thick mineral oil layer. It shields from radioactivity of photomultipliers (PMTs) and of the surrounding rock, and is one of the major improvements over the CHOOZ experiment [4]. 390 10-inch PMTs [30–32] are installed on the stainless steel buffer tank inner wall to collect light from the inner volumes. These three volumes and the PMTs constitute the inner detector (ID).

Outside the ID, and optically separated from it, is a 50 cm thick “inner veto” liquid scintillator (IV). It is equipped with 78 8-inch PMTs and functions as a cos-

mic muon veto and as a shield to spallation neutrons produced outside the detector. The detector is surrounded by 15 cm of demagnetized steel to suppress external γ -rays. The main detector is covered by an outer veto system (not used in this analysis).

The readout is triggered by custom energy sum electronics [33–35]. The ID PMTs are separated into two groups of 195 PMTs uniformly distributed throughout the volume and the PMT signals in each group are summed. The signals of the IV PMTs are also summed. If any of the three sums is above a set energy threshold, the detector is read out with 500 MHz flash-ADC electronics [36, 37] with customized firmware and a deadtime-free acquisition system. Upon each trigger, a 256 ns interval of the waveforms of both ID and IV signals is recorded. The low trigger rate (120 Hz) allowed the ID readout threshold to be set at 350 keV, well below the 1.02 MeV minimum energy of an IBD positron, greatly reducing the threshold systematics.

The experiment is calibrated by several methods. A multi-wavelength LED–fiber light injection system (LI) produces fast light pulses illuminating the PMTs from fixed positions. Radio-isotopes ^{137}Cs , ^{68}Ge , ^{60}Co , and ^{252}Cf were deployed in the target along the vertical symmetry axis and, in the gamma catcher, through a rigid loop traversing the interior and passing along boundaries with the target and the buffer. The detector was monitored using spallation neutron captures on H and Gd, residual natural radioactivity, and daily LI runs. The stability of the peak energy of neutron captures on Gd in IBD candidates is shown in Figure 2. The energy response was found to be stable within 1% over time.

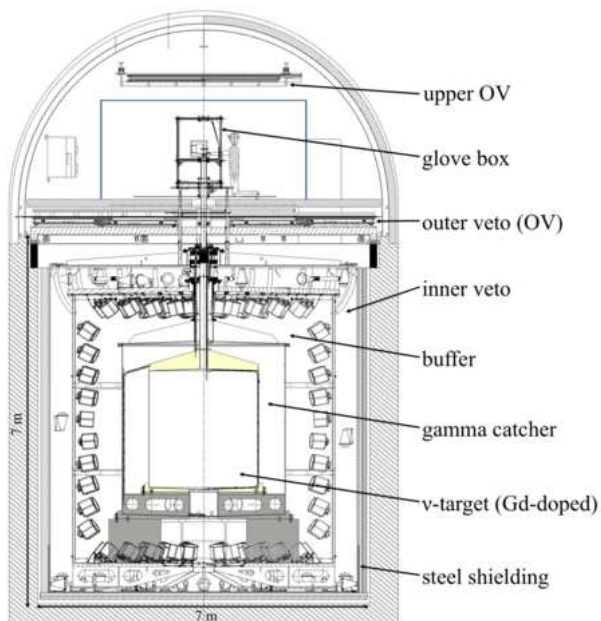


FIG. 1. A cross-sectional view of the Double Chooz detector system.

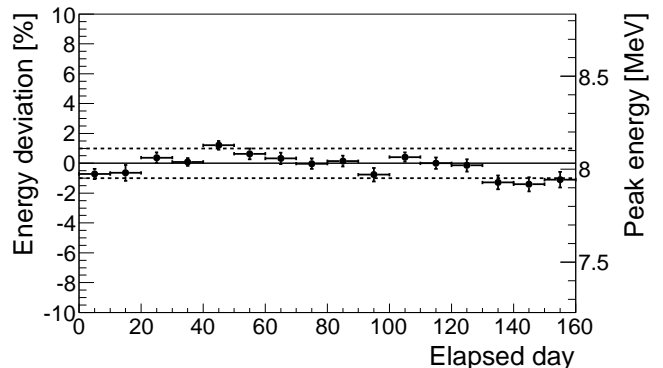


FIG. 2. The peak of the energy of neutron captures on Gd in IBD events(right scale) and its deviation from its average value(left scale) as a function of elapsed(calendar) day.

The signature of IBD events is a delayed coincidence between a prompt positron energy deposition, E_{prompt} , and a delayed energy deposition, E_{delay} , due to the neutron capture on H or Gd within Δt_{e+n} . The fiducial volume is constrained to the target vessel without position cuts by requiring a $\bar{\nu}_e$ event to have a capture on Gd, identified by its emission of ~ 8 MeV in γ rays. The

analysis compares the number and energy distribution of detected events to a prediction based on the reactor data.

Energy measurements are based on the total charge, Q_{tot} , collected by the PMTs and corrected for gain variations. The energy is reconstructed scaling Q_{tot} by a constant, adjusted so that the energy of the gamma emitted following neutron capture on H reconstructs to 2.22 MeV at the target center. This corresponds to ~ 200 pe/MeV. Our Monte Carlo (MC), based on GEANT4 [38], is used to model the detector response and to calculate its acceptance. It uses parameters for quenching [39], absorption, re-emission, refraction, etc. determined from laboratory measurements of the detector liquids. Comparisons between actual and simulated calibration data were used to develop a parametric function to correct the simulation, and to assess the uncertainties in the energy reconstruction. The function is a product of two factors. One, dependent on energy, ranges from 0.97 to 1.05 for 0.7-10.0 MeV. The other, dependent on position, ranges from 0.94 to 1.00 over the target volume.

The following criteria are applied to select $\bar{\nu}_e$ candidates. Triggers within a 1000 μ s window following a cosmic muon crossing the IV or the ID (46 s^{-1}) are rejected to limit spallation neutron and cosmogenic backgrounds. This requirement is followed by five selections: 1) a cut rejecting events caused by some sporadically glowing PMT bases, resulting in light localized to a few PMTs and spread out in time: $Q_{max}/Q_{tot} < 0.09$ (0.06) for the prompt (delayed) energy and $\text{rms}(t_{start}) < 40$ ns, where Q_{max} is the maximum charge recorded by a single PMT and $\text{rms}(t_{start})$ is the standard deviation of the times of the first pulse on each PMT; 2) $0.7 \text{ MeV} < E_{prompt} < 12.2 \text{ MeV}$; 3) $6.0 \text{ MeV} < E_{delay} < 12.0 \text{ MeV}$; 4) $2 \mu\text{s} < \Delta t_{e+n} < 100 \mu\text{s}$, where the lower cut eliminates correlated noise and the upper cut is determined by the $\sim 30 \mu\text{s}$ capture time on Gd; 5) a multiplicity cut to reject correlated backgrounds defined as no additional valid trigger from 100 μs preceding the prompt candidate to 400 μs after it. Applying selections (1-5) yields 4121 candidates or 42.6 ± 0.7 events/day, uniformly distributed within the target, for an analysis live time of 96.8 days.

Contributions from background events surviving these cuts have been estimated as follows. Uncorrelated coincidences result mainly from the random association of a prompt energy deposition due to radioactivity (7.6 s^{-1}) and a later candidate neutron capture ($\simeq 20/\text{hour}$). This background is measured by applying selection cuts (1-5) but modifying selection (4) such that the 2 – 100 μs time window is shifted by 1000 μs relative to the prompt trigger. To improve the precision of this background measurement, 198 such windows, each shifted from the previous one by 500 μs , were used, leading to 0.33 ± 0.03 events per day.

Fast neutrons induced by muons traversing the rock can interact in the target producing a recoil proton and, later, be captured, simulating an IBD event. We estimate this rate to be 0.83 ± 0.38 events per day (in-

cluding a contribution from stopping muons) by applying cuts (1-5), but modifying selection (2) such that $12.2 \text{ MeV} < E_{prompt} < 30 \text{ MeV}$, and then extrapolating to the signal region, assuming a flat energy spectrum. We account for an uncertainty in this extrapolation, and for the contribution of stopping muons, by including a shape error ranging up to $\pm 70\%$ of the flat extrapolation at lower energies.

${}^9\text{Li}$ β -n emitters are produced preferentially by energetic muons. They were studied by searching for a triple delayed coincidence between a muon depositing $> 600 \text{ MeV}$ in the detector and a $\bar{\nu}_e$ -like pair of events, where the delay between the muon and prompt event is dictated by the 178 ms ${}^9\text{Li}$ half-life, which precludes vetoing on all muons. Fitting the resulting time distribution with a flat component and an exponential with the ${}^9\text{Li}$ lifetime results in an estimated rate of 2.3 ± 1.2 events/day. This rate is assigned the energy spectrum of the ${}^9\text{Li}$ decay branches. A shape uncertainty of up to 20% is introduced to account for uncertainties in some decay branches. ${}^8\text{He}$ is not considered since it is less abundantly produced [40]. The total background rate, $3.46 \pm 1.26 \text{ d}^{-1}$, is summarized in Table I.

The overall background envelope is independently verified by analyzing 22.5 hours of both-reactors-off data (< 0.3 residual $\bar{\nu}_e$ events). Two $\bar{\nu}_e$ candidates, with prompt energies of 4.8 MeV and 9.8 MeV, pass cuts (1-5). They were associated within 30 cm and 220 ms with the closest energetic muon, and are thus likely to be associated with ${}^9\text{Li}$.

TABLE I. The breakdown of the estimated background rate. Additional shape uncertainties are described in the text.

Background	Rate/day	Syst. Uncertainty (% of signal)
Accidental	0.33 ± 0.03	< 0.1
Fast neutron	0.83 ± 0.38	0.9
${}^9\text{Li}$	2.3 ± 1.2	2.8

The following detector-related corrections and efficiencies as well as their uncertainties were evaluated using the MC. The energy response introduces a 1.7% systematic uncertainty determined from fits to calibration data. The number of free protons in the target scintillator, 6.747×10^{29} based on its weight measurement, has an uncertainty of 0.3%, originating from the knowledge of the scintillator hydrogen ratio. A dedicated simulation including molecular bond effects [41] indicates that the number of IBD events occurring in the gamma catcher with the neutron captured in the target (spill in) exceeds the number of events in the target with the neutron escaping to the gamma catcher (spill out) by $1.4\% \pm 0.4\%$, 0.8% lower than our standard MC prediction which was therefore reduced accordingly. Above the 700 keV analysis threshold, the trigger efficiency is $100.0_{-0.4}^{+0}\%$, assessed with a low threshold prescaled trigger. Calibration data taken with the ${}^{252}\text{Cf}$ source were used to check the MC for any biases in the neutron selection criteria

and estimate their contributions to the systematic uncertainty. The fraction of neutron captures on Gd is found to be $(86.0 \pm 0.5)\%$ near the center of the target, 2.0% lower than the simulation prediction which was reduced accordingly with a relative systematic uncertainty of 0.6%. The simulation reproduces the 96.5% efficiency of the Δt_{e+n} cut with an uncertainty of 0.5% and the 94.5% fraction of neutron captures on Gd accepted by the 6.0 MeV cut with an uncertainty of 0.6%. The MC normalization was adjusted for the muon veto (-4.5%) and the multiplicity veto (-0.5%) dead-times.

TABLE II. Contributions of the detector and reactor errors to the absolute normalization systematic uncertainty.

Detector		Reactor	
Energy response	1.7%	Bugey4 measurement	1.4%
E_{delay} Containment	0.6%	Fuel Composition	0.9%
Gd Fraction	0.6%	Thermal Power	0.5%
Δt_{e+n}	0.5%	Reference Spectra	0.5%
Spill in/out	0.4%	Energy per Fission	0.2%
Trigger Efficiency	0.4%	IBD Cross Section	0.2%
Target H	0.3%	Baseline	0.2%
Total	2.1%	Total	1.8%

The full covariance matrix of the emitted $\bar{\nu}_e$ spectra was computed as prescribed in [27]. MURE provided the fractions of fissions per isotope $^{235}\text{U}=48.8\%$, $^{239}\text{Pu}=35.9\%$, $^{241}\text{Pu}=6.7\%$, and $^{238}\text{U}=8.7\%$ and the fission rate covariance matrix. The resulting relative uncertainties on the above fission fractions are $\pm 3.3\%$, $\pm 4\%$, $\pm 11.0\%$ and $\pm 6.5\%$, respectively. The error associated with the thermal power is $\pm 0.46\%$ at full power [42, 43], fully correlated between the two cores.

To avoid being affected by possible very short baseline $\bar{\nu}_e$ oscillations [4, 44, 45], we adopt the reactor $\bar{\nu}_e$ spectrum of [23, 27], but the global normalization is fixed by the Bugey4 rate measurement [46] with its associated 1.4% uncertainty. A relative correction of $(0.9 \pm 1.3\%)$ of the Bugey4 value accounts for the difference in core inventories. The IBD differential cross section is taken from [47], using 881.5 ± 1.5 s [1] as the neutron lifetime. The systematic uncertainties are summarized in Table II. The expected no-oscillation number of $\bar{\nu}_e$ candidates is 4344 ± 165 , including background.

The measured daily rate of IBD candidates as a function of the no-oscillation expected rate for different reactor power conditions is shown in Figure 3. The extrapolation to zero reactor power of the fit to the data (including the both-reactors-off) yields 3.2 ± 1.3 events per day, in excellent agreement with our background estimate and the both-reactors-off data.

Our measurement can be expressed as an observed IBD cross section per fission, σ_f^{DC} , a quantity which depends on the number of events observed, the number of target protons, the detector efficiency, the number of fissions occurring during our measurement and the distance to the reactors, yielding $\sigma_f^{DC} = (5.383 \pm 0.210) 10^{-43}$ cm²/fission. The Bugey4

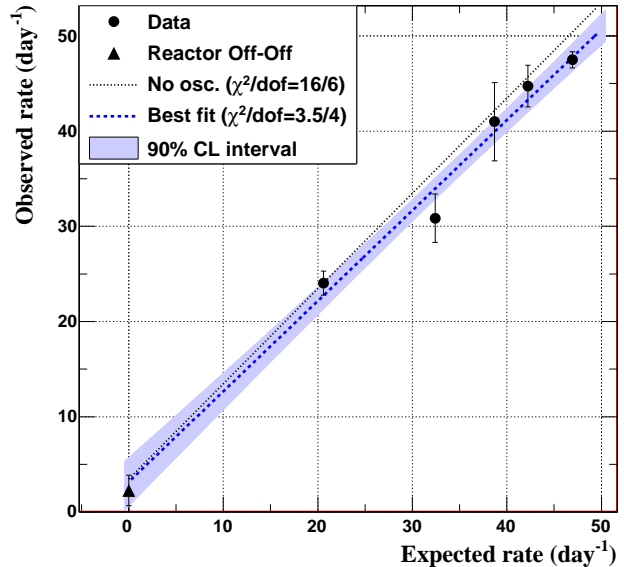


FIG. 3. Daily number of $\bar{\nu}_e$ candidates as a function of the expected number of $\bar{\nu}_e$. The dashed line is a fit to the data, the band is the 90% C.L. of this fit. The dotted line is the expectation in the no-oscillation scenario. The triangle indicates the measurement with both reactors off.

measurement, corrected to match our fractions of isotopes quoted above, yields a cross section per fission of $(5.703 \pm 0.108) 10^{-43}$ cm²/fission. The ratio of these two measurements is independent of any possible very short baseline oscillations. (Without Bugey4 normalization, the prediction, for our running conditions and using the reference spectra [23, 27], is $(6.209 \pm 0.170) 10^{-43}$ cm²/fission).

The ratio of observed to expected events is $R_{DC} = 0.944 \pm 0.016$ (stat) ± 0.040 (syst), corresponding to $\sin^2 2\theta_{13} = 0.104 \pm 0.030$ (stat) ± 0.076 (syst) for $\Delta m_{13}^2 = 2.4 \times 10^{-3}$ eV².

The analysis is improved by comparing the positron spectrum in 18 variably sized energy bins between 0.7 and 12.2 MeV to the expected number of $\bar{\nu}_e$ events, again using $\Delta m_{13}^2 = 2.4 \times 10^{-3}$ eV². The analysis, performed with a standard χ^2 estimator, uses four covariance matrices to include uncertainties in the antineutrino signal, detector response, signal and background statistics, and background spectral shape. With very few positrons expected above 8 MeV, the region 8–12.2 MeV reduces the uncertainties in the correlated backgrounds with some additional contribution to the statistical uncertainty.

The best fit results in $\sin^2 2\theta_{13} = 0.086 \pm 0.041$ (stat) ± 0.030 (syst) with a χ^2/DOF of 23.7/17, whereas the $\sin^2 2\theta_{13} = 0.0$ hypothesis results in a χ^2/DOF of 26.6/18. Using a frequentist approach [48] we find an allowed region of $0.017 < \sin^2 2\theta_{13} < 0.16$ at 90% CL, and exclude the no

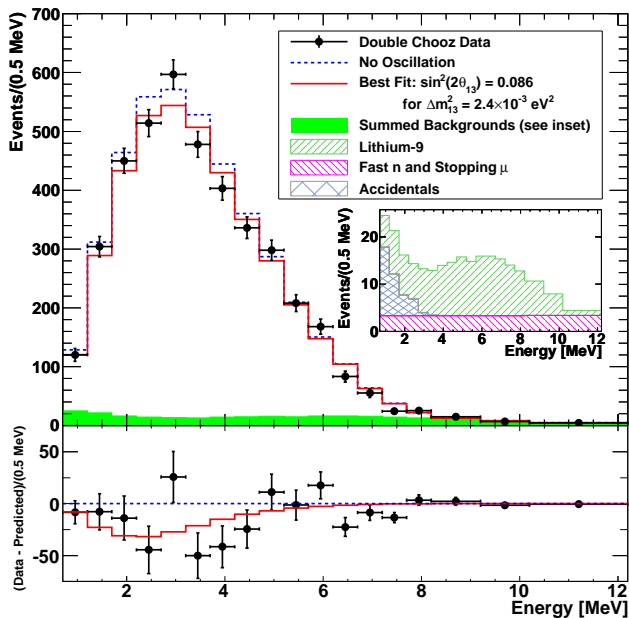


FIG. 4. Top: Expected prompt energy spectra, including backgrounds, for the no-oscillation case and for the best fit $\sin^2 2\theta_{13}$, superimposed on the measured spectrum. Inset: stacked histogram of backgrounds. Bottom: Difference between data and the no-oscillation spectrum (data points) and difference between the best fit and no-oscillation expectations (curve)

oscillation hypothesis at the 94.6% C.L.

We determine our best estimate of the $\bar{\nu}_e$ and background rates with a pulls-based approach [49], the results of which are shown in Table III. From the best fit we obtain a contribution from ${}^9\text{Li}$ reduced by $\sim 19\%$, and with an uncertainty decreased from 52% to 26%. The fast neutron value is decreased by 5% with almost unchanged uncertainty.

TABLE III. Summary of the effect of a pulls term approach on the fast neutron and ${}^9\text{Li}$ backgrounds and on the energy scale. Uncertainty values are in parentheses.

	Fast n. Bkg(%)	${}^9\text{Li}$ (%)	Escale (value)
Rate only	100 (46)	100 (52)	0.997 (0.007)
Rate + Shape	95.2 (38)	81.5 (25.5)	0.998 (0.005)

Figure 4 shows the measured positron spectrum superimposed on the expected spectra for the no-oscillation hypothesis and for the best fit (including fitted backgrounds).

Combining our result with the T2K [11] and MINOS [12] measurements leads to $0.003 < \sin^2 2\theta_{13} < 0.219$ at the 3σ level.

In summary, Double Chooz has searched for $\bar{\nu}_e$ disappearance using a 10 m^3 detector located 1050 m from two reactors. A total of 4121 events were observed where 4344 ± 165 were expected for no-oscillation, with a signal to background ratio of $\approx 11:1$. In the context of neutrino oscillations, this deficit leads to $\sin^2 2\theta_{13} = 0.086 \pm 0.041$ (stat) ± 0.030 (syst), based on an analysis using rate and energy spectrum information. The no-oscillation hypothesis is ruled out at the 94.6% C.L. Double Chooz continues to run, to reduce statistical and background systematic uncertainties. A near detector will soon lead to reduced reactor and detector systematic uncertainties and to an estimated 1σ precision on $\sin^2 2\theta_{13}$ of ~ 0.02 .

We thank all the technical and administrative people who helped build the experiment and the CCIN2P3 computer center for their help and availability. We thank, for their participation, the French electricity company EDF, the European fund FEDER, the Région de Champagne Ardenne, the Département des Ardennes and the Communauté des Communes Rives de Meuse. We acknowledge the support of CEA and CNRS/IN2P3 in France, MEXT and JSPS of Japan, the Department of Energy and the National Science Foundation of the United States, the Ministerio de Ciencia e Innovación (MICINN) of Spain, the Max Planck Gesellschaft and the Deutsche Forschungsgemeinschaft DFG (SBH WI 2152), the Transregional Collaborative Research Center TR27, the Excellence Cluster "Origin and Structure of the Universe" and the Maier-Leibnitz-Laboratorium Garching, the Russian Academy of Science, the Kurchatov Institute and RFBR (the Russian Foundation for Basic Research), the Brazilian Ministry of Science, Technology and Innovation (MCTI), the Financiadora de Estudos e Projetos (FINEP), the Conselho Nacional de Desenvolvimento Científico e Tecnológico (CNPq), the São Paulo Research Foundation (FAPESP) and the Brazilian Network for High Energy Physics (RENAFAE) in Brazil.

[1] K. Nakamura et al., J. Phys. G **37**, 075021 (2010).
[2] B. Pontecorvo, JETP **34**, 172 (1958).
[3] Z. Maki, M. Nakagawa, and S. Sakata, Prog. Theor. Phys. **28**, 870 (1962).
[4] M. Appolonio et al., Phys. Lett. **B466**, 415 (1999).
[5] F. Boehm et al., Phys. Rev. Lett. **84**, 3764 (2000).
[6] H. Minakata, H. Sugiyama, O. Yasuda, K. Inoue, and F. Suekane, Phys. Rev. D **68**, 033017 (2003), URL <http://link.aps.org/doi/10.1103/PhysRevD.68.033017>.
[7] H. Minakata, H. Sugiyama, O. Yasuda, K. Inoue,

and F. Suekane, Phys. Rev. D **70**, 059901 (2004), URL <http://link.aps.org/doi/10.1103/PhysRevD.70.059901>.
[8] P. Adamson et al. (MINOS Collaboration), Phys. Rev. Lett. **106**, 181801 (2011).
[9] X. Guo et al. (Daya Bay Collaboration) (2006), arXiv:hep-ex/0701029.
[10] J. K. Ahn et al. (RENO Collaboration) (2010), arXiv:hep-ex/1003.1391.
[11] K. Abe et al. (T2K Collaboration), Phys. Rev. Lett. **107**, 041801 (2011).

- [12] P. Adamson et al., Phys. Rev. Lett. **107**, 181802 (2011), hep-ex/1108.0015v1.
- [13] T. Schwetz et al. (2011), arXiv:hep-ph/1108.1376v1.
- [14] G. L. Fogli et al. (2011), arXiv:hep-ph/1106.6028v2.
- [15] F. Ardellier et al. (Double Chooz Collaboration) (2006), hep-ex/0606025v4.
- [16] G. Mention, Ph.D. thesis (2005), URL <http://tel.archives-ouvertes.fr/tel-00010528/fr/>.
- [17] O. Meplan, Tech. Rep. LPSC 0912 and IPNO-09-01 (2009).
- [18] MURE, *Mcnp utility for reactor evolution: couples monte-carlo transport with fuel burnup calculations* (2009), URL <http://www.nea.fr/tools/abstract/detail/nea-1845>.
- [19] R. R. G. Marleau and A. Hebert, Tech. Rep. IGE-157 (1994).
- [20] C. Jones et al. (2011), arXiv:nucl-ex/1109.5379v1.
- [21] V. Kopeikin et al., *Reactor as a source of antineutrinos: Thermal fission energy* (2004), hep-ph/0410100v1.
- [22] *Jeff and eff projects* <http://www.oecd-nea.org/dbdata/jeff/>, URL <http://www.oecd-nea.org/dbdata/jeff/>.
- [23] P. Huber, Phys. Rev. C **84**, 024617 (2011).
- [24] W. G. K. Schreckenbach, G. Colvin and F. von Feilitzsch, Phys. Lett. B **160** (1985).
- [25] A. F. von Feilitzsch and K. Schreckenbach, Phys. Lett. B **118** (1982).
- [26] A. A. Hahn et al., Phys. Lett. B **218** (1989).
- [27] T. Mueller et al., Phys. Rev. C **83**, 054615 (2011).
- [28] C. Aberle et al., *Large scale gadolinium-beta-diketonate based organic liquid scintillator production for antineutrino detection*. (2011), arXiv:1112.5941. Submitted to JINST.
- [29] C. Aberle et al., Chem. Phys. Lett. **516**, 257 (2011).
- [30] T. Matsubara et al., Nucl. Instrum. Meth. in Physics Research **A661**, 16 (2011), 1104.0786[phys.ins-det].
- [31] C. Bauer et al., JINST **6**, P06008 (2011), 1104.0758.
- [32] E. Calvo et al., Nucl. Instrum. Meth. in Physics Research **A621**, 222 (2010), 0905.3246[phys.ins-det].
- [33] C. Kuhnt, Master's thesis (2010), URL http://www.physik.rwth-aachen.de/fileadmin/user_upload/www_
- [34] F. Beissel et al., *The trigger and timing system of the double chooz experiment. in preparation*.
- [35] B. Reinhold, Ph.D. thesis, RWTH Aachen University (2009).
- [36] A. Cabrera et al., Nucl. Instrum. Meth. in Physics Research **A617**, 473 (2010).
- [37] T. Akiri, Ph.D. thesis (2010), URL <http://tel.archives-ouvertes.fr/tel-00580175/fr/>.
- [38] S. Agostinelli et al., Nucl. Instrum. Meth. in Physics Research **A506**, 250 (2003).
- [39] C. Aberle et al., JINST **6**, P11006 (2011).
- [40] S. Abe et al., Phys. Rev. C **81**, 025807 (2010).
- [41] J. P. Both et al., Tech. Rep. CEA-REPORT: CEA-R-6044, DTI, CEA/Saclay, France (2003).
- [42] S. F. E. Tournu et al., EPRI 2001.1001470, Palo Alto, CA. (2001).
- [43] Standard AFNOR XP X 07-020, Palo Alto, CA. (1996).
- [44] G. Mention et al., Phys. Rev. D **83**, 073006 (2011).
- [45] C. Giunti and M. Laveder (2011), hep-ph/1111.5211v2.
- [46] Y. Declais et al., Phys. Lett. **B338**, 383 (1994).
- [47] P. Vogel and J. F. Beacom, Phys. Rev. D **60**, 053003 (1999).
- [48] G. J. Feldman and R. D. Cousins, Phys. Rev. D **57**, 3873 (1998).
- [49] D. Stump et al., Phys. Rev. D **65**, 014012 (Appendix B) (2001).